JCTC Journal of Chemical Theory and Computation

The Rotational *g* Tensor as a Benchmark for Density-Functional Theory Calculations of Molecular Magnetic Properties

David J. D. Wilson,*,† Chris E. Mohn, and Trygve Helgaker

Department of Chemistry, University of Oslo, P. O. Box 1033 Blindern, N-0315 Oslo, Norway

Received April 15, 2005

Abstract: The rotational *g* factor for a large number of organic compounds has been investigated with density-functional theory. Rapid convergence toward the basis-set limit is ensured by the use of London atomic orbitals. A statistical analysis of the results has been carried out in comparison with accurate experimental data. It is shown that gradient-corrected and hybrid functionals reproduce experimental results most closely, with the Keal−Tozer KT2 functional being the most accurate.

I. Introduction

Calculations of rotational *g* tensors constitute a particular challenge to ab initio theory, with the errors introduced in the description of the electronic system often being much larger than the experimental standard deviations obtained in highly accurate molecular−beam[1] and microwave Zeeman experiments.[2,3] Still, theoretical studies of the rotational *g* tensor have been presented at various levels of ab initio theory, including Hartree−Fock theory,[4−6] second-order Møller−Plesset (MP2) theory,[7−9] linearized coupled-cluster doubles theory,[9] the second-order polarization propagator approximation,[10−12] multiconfigurational self-consistent field (MCSCF) theory,[13−15] and, for small systems, full configuration-interaction theory.[16,17] However, although the results presented in these wave-function studies are mostly in qualitative agreement with experimental results, they often differ by more than 10 experimental standard deviations from the experimental values, especially at lower levels of theory.

In recent years, density-functional theory (DFT) has emerged as the most popular quantum-mechanical method for studying molecular properties. While the standard local-density approximation (LDA) Slater−Vosko−Wilk−Nusair (SVWN) functional[18] typically gives results of intermediate quality, generalized gradient approximation (GGA) functionals such as the Becke−Lee−Yang−Parr (BLYP) functional[19,20] and hybrid functionals such as the Becke three-parameter Lee−Yang−Parr (B3LYP) functional[21−23] often describe electron correlation effects of molecular properties with an accuracy comparable to that of MP2[24] and coupled-cluster single-and-doubles[25−27] theories. In view of the accurate experimental measurements of *g* tensors, it is therefore of considerable interest to apply DFT to the calculation of this property and, in particular, to benchmark DFT *g* tensors against the available experimental data.

In common with all properties that involve interactions with an external magnetic field, the calculation of rotational *g* factors suffers from the gauge-origin problem and slow basis-set convergence. Despite the many treatments of the gauge-origin problem proposed over the years,[10,28−34] it was, in principle, already solved in 1937 by London, who proposed attaching field-dependent complex phase factors to the atomic orbitals.[35] In London's scheme, each atomic orbital has its own gauge origin: the nucleus to which it is attached. These London orbitals, which are also known as gauge invariant atomic orbitals, are correct to the first order in the magnetic field for a one-electron, one-center problem.[36] Their use in ab initio theory was pioneered by Hameka[37−39] in the 1950s and 1960s and by Ditchfield[40] in the 1970s, but the efficient implementation of London orbitals was not achieved until the 1990s, with the work of Wolinski and co-workers.[41] London orbitals are now widely used in quantum chemistry, with Hartree−Fock,[42] MP2,[43] MCSCF,[44] and

* Corresponding author phone: +47 228 55432; fax: +47 228 55441; e-mail: d.j.wilson@kjemi.uio.no.

† Current affiliation: Chemistry Department, La Trobe University, Australia.

10.1021/ct050101t CCC: $30.25
Published on Web 08/16/2005

Table 1. List of Molecules Considered in This Study[a]

Linear Molecules			
carbonyl sulfide[b]	OCS	hydrogen cyanide	$HC^{15}N$
hydrogen boron sulfide[c]	HBS	fluoro cyanide[d]	$FC^{15}N$
carbonyl selenide[e,f]	OCSe	chloro cyanide[g,d]	$ClC^{15}N$
carbon monoxide	CO	bromo cyanide[d]	$BrC^{15}N$
carbon sulfide	CS	fluoro acetylene[h]	HCCF
carbon selenide[i]	CSe	chloro acetylene[j,h]	HCCCl
methylidene phosphine[k,c]	HCP	bromo acetylene[l,h]	HCCBr
nitrous oxide[m]	N_2O		
Symmetric Top Compounds			
acetonitrile	CH_3CN	fluoromethane	CH_3F
methylisocyanide	CH_3NC[n]	chloromethane	CH_3Cl
ammonia	NH_3	trifluoromethane	CHF_3
Nonring Planar Asymmetric Tops			
2-methyl but-1,3-diene	C_5H_8	difluoromethane	CH_2F_2
acrolein	C_3H_4O	carbonic dufluoride[o]	F_2CO
propene[p]	C_3H_6	formyl fluoride[q]	HFCO
propynal[r]	C_3H_2O	fluoroethylene	C_2H_3F
dimethyl ether	C_2H_6O	1,1-difluoro ethylene	$C_2H_2F_2$
dimethyl sulfide	C_2H_6S	*cis*-difluoro ethylene[r]	$C_2H_2F_2$
acetaldehyde	C_2H_4O	trifluoro ethene[s]	C_2HF_3
formaldehyde[p]	H_2CO	fluoro ethane[o]	C_2H_5F
thioformaldehyde	H_2CS	ozone[s,t]	O_3
formic acid	HCOOH	sulfur dioxide[u]	SO_2
formamide	$HCONH_2$	difluoro oxide	OF_2
glycoaldehyde[r]	$C_2H_4O_2$	hypofluoros acid	HOF
methyl formate	$C_2H_4O_2$	water	H_2O
ketene	$C_2H_2O_2$	hydrogen sulfide	H_2S
Three-Member Ring Compounds			
methylene cyclopropane	C_4H_6	thiirane	C_2H_4S
cyclopropene	C_3H_4	cyclopropenone[v]	C_3H_2O
aziridine	C_2H_5N	methyl cyclopropene	C_4H_6
oxirane	C_2H_4O		
Four-Member Ring Compounds			
cyclobutene	C_4H_6	oxetan	C_4H_6O
oxetane	C_3H_6O	β-pripiolactone	$C_3H_4O_2$
methylene cyclobutane	C_5H_8	diketene	$C_4H_4O_2$

[a] Experimental *g*-tensor data taken from ref 3 except where noted. Experimental geometries taken from ref 68 unless noted. [b] Experimental data from ref 63. Three isotopes considered ($^{16}O^{12}C^{32}S$,-$^{16}O^{12}C^{34}S$, and $^{16}O^{13}C^{32}S$). [c] Geometry from ref 72. [d] Geometry from ref 69. [e] Two isotopes considered ($OC^{76}Se$ and $OC^{80}Se$). [f] Geometry from ref 70. [g] Experimental data from ref 66. [h] Geometry from ref 73. [i] Geometry from ref 71. [j] Two isotopes considered ($^{35}ClCCH$ and $^{37}ClCCH$). [k] Two isotopes considered (HCP and DCP). [l] Two isotopes considered ($^{79}BrCCH$ and $^{81}BrCCH$). [m] Two isotopes considered ($^{15}N_2O$ and $^{14}N_2O$). [n] Geometry from ref 74. [o] Geometry from ref 75. [p] Geometry from ref 14. [q] Geometry from ref 77. [r] Geometry from ref 76. [s] Geometry from ref 78. [t] Experimental data from ref 65. [u] Experimental data from ref 64. [v] Geometry from ref 79.

coupled-cluster[45−47] implementations reported. Particularly impressive is the rapid basis-set convergence of magnetic properties with the use of London orbitals.[5]

To date, very few DFT studies of rotational *g* tensors have been reported,[48] only one of which (from our laboratory) uses London orbitals.[49] Here, we present London DFT calculations of the rotational *g* tensor for the 61 organic molecules listed in Table 1. These molecules differ in the importance and relative magnitudes of static and dynamic electron correlation; hence, they constitute a suitable set for testing the accuracy of various computational approaches in the calculation of *g* tensors. To benchmark the performance of the various density functionals, a statistical analysis of the calculated *g* tensors is carried out, comparing against experimental data taken almost exclusively from the reviews of Flygare and co-workers.[2,3] In all calculations, we use a very recent London orbital implementation of DFT magnetic properties in DALTON.[50]

The paper is organized as follows: In Section 2, we outline the theory of *g*-tensor calculations, with some computational details given in Section 3. In Section 4, the results and statistical analysis from the calculations are presented. Some concluding remarks are given in Section 5.

II. Theory

In an applied external magnetic field, the rotational energy levels of a rotating molecule are shifted relative to those in the absence of such a field. These shifts, which arise from the Zeeman interaction of the external magnetic induction **B** with the magnetic dipole moment generated by the rotating molecule of angular momentum **J** in the center-of-mass coordinate system, are conventionally represented as

$$\Delta E = -\mu_N \mathbf{B}^T \mathbf{g} \mathbf{J}, \tag{1}$$

where the three-by-three matrix **g** is the rotational *g* tensor and μ_N is the nuclear magneton. For computational purposes, it is convenient to express the *g* tensor as a derivative of the molecular electronic energy $\epsilon(\mathbf{B},\mathbf{J})$ with respect to the magnetic field strength and the rotational angular momentum at $\mathbf{B} = \mathbf{0}$ and $\mathbf{J} = \mathbf{0}$:[5]

$$\mathbf{g} = -\frac{\hbar}{\mu_N} \frac{\partial^2 \epsilon(\mathbf{B},\mathbf{J})}{\partial \mathbf{B} \partial \mathbf{J}}\bigg|_{\mathbf{B},\mathbf{J}=\mathbf{0}}. \tag{2}$$

In this manner, the rotational *g* tensor may be obtained in the same way as any other time-independent second-order molecular property, once the expression for $\epsilon(\mathbf{B},\mathbf{J})$ (including the purely nuclear interactions) has been set up for a rotating molecular system in the presence of an external magnetic field. In principle, this is a straightforward process once the expression for the Hamiltonian has been written down.

For a rotating molecule in an external magnetic field, we can write down the Hamiltonian in the center-of-mass (CM) coordinate system as

$$H(\mathbf{B},\mathbf{J}) = H_0 + \frac{1}{2}\mathbf{L}_O\mathbf{B}^T - \mathbf{L}_{CM}^T \mathbf{I}_{nuc}^{-1}\mathbf{J} + \frac{1}{2}\mathbf{B}^T\sum_i(\mathbf{r}_i^T\mathbf{R}_O\mathbf{I}_3 - \mathbf{r}_i\mathbf{R}_O^T)\mathbf{I}_{nuc}^{-1}\mathbf{J} - \frac{1}{2}\mathbf{B}^T\sum_K Z_K(\mathbf{R}_K^T\mathbf{R}_K\mathbf{I}_3 - \mathbf{R}_K\mathbf{R}_K^T)\mathbf{I}_{nuc}^{-1}\mathbf{J} \tag{3}$$

where the first term H_0 is the spin-free nonrelativistic electronic Hamiltonian of a nonrotating diamagnetic molecule in the absence of an external magnetic field. The remaining four terms in $H(\mathbf{B},\mathbf{J})$ are either linear (paramagnetic) or bilinear (diamagnetic) in **B** and **J**. The first paramagnetic term, $^1/_2\mathbf{L}_O\mathbf{B}^T$, where $\mathbf{L}_O$ is the angular momentum operator

of the electrons about the origin $\mathbf{R}_O$ of the external potential $\mathbf{A}(\mathbf{r}) = {}^1/_2\mathbf{B} \times (\mathbf{r} - \mathbf{R}_O)$

$$\mathbf{L}_O = \sum_i (\mathbf{r}_i - \mathbf{R}_O) \times \nabla_i \tag{4}$$

represents the Zeeman interaction of the electrons with the magnetic induction $\mathbf{B}$. In the same manner, the second paramagnetic term $-\mathbf{L}_{CM}^T \mathbf{I}_{nuc}^{-1}\mathbf{J}$ in eq 3, where $\mathbf{I}_{nuc}$ is the moment-of-inertia tensor and $\mathbf{L}_{CM}$ is the electronic angular-momentum operator in the center-of-mass coordinate system

$$\mathbf{L}_{CM} = \sum_i \mathbf{r}_i \times \nabla_i \tag{5}$$

represents the Zeeman interaction of the electrons with the magnetic field $-2\mathbf{I}_{nuc}^{-1}\mathbf{J}$ generated by the rotating molecule. Finally, of the two diamagnetic terms in the Hamiltonian, eq 3, the first involves the electrons and, therefore, enters a one-electron expectation value; the second is a purely nuclear operator whose contribution to the g tensor does not depend on the electronic state. Note that, in $H(\mathbf{B},\mathbf{J})$, we have excluded all terms that do not contribute to the rotational g tensor—for example, the diamagnetic term quadratic in $\mathbf{B}$.

For the calculation of rotational g tensors, the use of London orbitals has been demonstrated not only to ensure gauge-origin independent results but also to accelerate the convergence toward the basis-set limit (compared to conventional field-independent orbitals).[35,36] The London atomic orbitals are here defined as

$$\omega_\mu(\mathbf{B},\mathbf{J}) = \exp[-i(\mathbf{A}_\mu^{\mathbf{B}} + \mathbf{A}_\mu^{\mathbf{J}})\mathbf{r}]\,\chi_\mu \tag{6}$$

with phase factors given by

$$\mathbf{A}_\mu^{\mathbf{B}} = \frac{1}{2}\mathbf{B} \times (\mathbf{R}_\mu - \mathbf{R}_O) \tag{7}$$

$$\mathbf{A}_\mu^{\mathbf{J}} = -\mathbf{I}_{nuc}^{-1}\mathbf{J} \times \mathbf{R}_\mu \tag{8}$$

where $\mathbf{R}_\mu$ is the position of the conventional atomic orbital χ_μ. Note that these orbitals, which are sometimes referred to as rotational London orbitals, constitute a generalization of the standard London orbitals, depending on $\mathbf{A}_\mu^{\mathbf{J}}$ as well as on $\mathbf{A}_\mu^{\mathbf{B}}$.[5] With these orbitals and the Hamiltonian (eq 3), one can derive the expressions for the g tensor using the machinery of time-independent response-theory described elsewhere.[51] The resulting expression for the rotational g tensor contains no reference to the gauge origin of the vector potential representing the external magnetic field but does depend correctly on the center of mass of the molecular system.

We here note the close relationship of the rotational g tensor to the molecular magnetizability, which represents the second derivative of the molecular energy with respect to an external magnetic field at $\mathbf{R} = \mathbf{0}$:

$$\xi = -\mu_0 \left.\frac{\partial^2 \epsilon(\mathbf{B})}{\partial \mathbf{B}^2}\right|_{\mathbf{B}=\mathbf{0}}. \tag{9}$$

In the center-of-mass coordinate system with $\mathbf{R}_{CM}$ as the chosen gauge origin of $\mathbf{L}_O$ in eq 3, the relationship between rotational g tensors and molecular magnetizabilities may be written as[5]

$$\mathbf{g} = -4m_p(\xi^{LAO} - \xi_{CM}^{dia})\mathbf{I}_{nuc}^{-1} + \frac{1}{2\mu_N}\sum_K Z_K(\mathbf{R}_K^T\mathbf{R}_K\mathbf{I}_3 - \mathbf{R}_K\mathbf{R}_K^T)\mathbf{I}_{nuc}^{-1} \tag{10}$$

where m_p is the proton mass, ξ^{LAO} is the magnetizability calculated with London orbitals, and ξ_{CM}^{dia} is the diamagnetic contribution to the magnetizability tensor, calculated using conventional orbitals with the gauge origin at the molecular center of mass. Hence, the rotational g tensor may be programmed and calculated as a simple extension to any code that already calculates the molecular magnetizability.

The extension of a Hartree−Fock magnetizability program to calculate DFT magnetizabilities and rotational g tensors is straightforward. The magnetizability, eq 9, may be calculated using standard response theory.[44] Parametrizing the electronic energy $\epsilon(\mathbf{B},\kappa)$ in terms of the orbital-rotation parameters κ (one parameter κ_{ai} for each pair of occupied and unoccupied orbitals), we then make use of the fact that the optimized electronic energy $\epsilon(\mathbf{B}) = \min_\kappa \epsilon(\mathbf{B},\kappa)$ is variational with respect to rotations between all pairs of occupied and virtual orbitals κ_{ai}, for all values of $\mathbf{B}$:[52−54]

$$\frac{\partial \epsilon(\mathbf{B},\kappa)}{\partial \kappa_{ai}} = \mathbf{0}, \text{ all values of } \mathbf{B} \tag{11}$$

The resulting expression for ξ in eq 9 then follows by differentiation and use of the chain rule:

$$\xi = -\mu_0 \frac{\partial^2 \epsilon(\mathbf{B},\kappa)}{\partial \mathbf{B}^2} - \mu_0 \sum_{ai} \frac{\partial^2 \epsilon(\mathbf{B},\kappa)}{\partial \mathbf{B}\partial \kappa_{ai}} \frac{\partial \kappa_{ai}}{\partial \mathbf{B}} \tag{12}$$

where all derivatives are evaluated at $\mathbf{B} = \mathbf{0}$. The first-order response of the wave function is evaluated from the linear set of equations

$$\sum_{bj} \frac{\partial^2 \epsilon(\mathbf{B},\kappa)}{\partial \kappa_{ai}\partial \kappa_{bj}} \frac{\partial \kappa_{bj}}{\partial \mathbf{B}} = -\frac{\partial^2 \epsilon(\mathbf{B},\kappa)}{\partial \kappa_{ai}\partial \mathbf{B}} \tag{13}$$

obtained by differentiation of the variational conditions, eq 13, with respect to $\mathbf{B}$. In eq 12, the first term is known as the diamagnetic part of the magnetizability and the second term, which contains the response of the wave function to the external magnetic field, is known as the paramagnetic part. The summations are over pairs of virtual and occupied orbitals, with κ_{ai} and κ_{bj} denoting the orbital-rotation parameters as discussed in refs 52−54. Equation 13 is similarly required for the calculation of chemical shieldings and magnetizabilities,[55,56] so a program with these properties implemented only requires the diamagnetic component of the magnetizability (and rotational g tensor) to be coded. The resulting DFT implementation, including the differentiation of London atomic orbitals, follows that for Hartree−Fock theory, which is outlined elsewhere.[44]

III. Computational Details

The above theory for the calculation of molecular magnetizabilities and rotational g tensors has recently been

Table 2. Errors of Calculated *g* Tensors Compared to Experimental Data

	optimized geometry		exptl geometry		optimized geometry		exptl geometry	
method	DZ	TZ	DZ	TZ	DZ	TZ	DZ	TZ
	Mean Relative Deviation, $\bar{\Delta}$				Mean Absolute Deviation, $\bar{\Delta}_{abs}$			
HF	0.005	0.002	−0.005	−0.005	0.029	0.028	0.038	0.036
LDA	−0.020	−0.016	−0.020	−0.014	0.027	0.023	0.028	0.023
BLYP	−0.016	−0.018	−0.014	−0.014	0.017	0.019	0.016	0.015
B3LYP	−0.011	−0.013	−0.009	−0.010	0.014	0.014	0.013	0.012
KT1	−0.006	−0.008	−0.005	−0.005	0.010	0.011	0.010	0.010
KT2	−0.004	−0.006	−0.002	−0.002	0.009	0.010	0.008	0.008
KT3	−0.005	−0.008	−0.003	−0.003	0.010	0.011	0.009	0.009
	Standard Deviation of Errors, $\bar{\Delta}_{std}$				Percentage Mean Absolute Deviation, $\bar{\Delta}_{pabs}$			
HF	0.145	0.141	0.240	0.235	21.1	18.2	21.5	19.1
LDA	0.093	0.075	0.101	0.080	15.3	16.1	14.7	14.1
BLYP	0.056	0.058	0.036	0.032	14.5	18.6	18.8	21.1
B3LYP	0.068	0.069	0.055	0.052	8.9	10.4	9.4	10.9
KT1	0.028	0.028	0.020	0.018	10.7	13.9	13.8	16.1
KT2	0.027	0.026	0.019	0.020	10.2	12.3	9.4	11.2
KT3	0.032	0.031	0.025	0.026	9.4	12.9	10.1	12.1

implemented in the DALTON program for DFT with London orbitals.[50] In this work, we have also taken the opportunity to implement the recently developed Keal−Tozer (KT) functionals KT1,[57] KT2,[58] and KT3,[59] with the implementations tested against CADPAC.[60] The KT functionals were included since they have previously been shown to provide accurate NMR shielding constants.[58]

To benchmark the implemented methods, we have carried out calculations of *g* tensors on a sample of 61 molecules (70 isotopes), representing 155 unique tensor elements. For all molecules, six density functionals were considered: the SVWN[18] functional of LDA theory; the BLYP,[19,20] KT1,[57] KT2,[58] and KT3[59] functionals of GGA theory; and the B3LYP[21−23] hybrid functional. Hartree−Fock results were included for comparison. To assess geometrical effects, the *g* tensors were calculated at both optimized and experimental molecular geometries. Experimental geometries were taken from the literature, with specific references given in Table 1. For a consistent and purely theoretical approach, we have calculated optimized geometries and rotational *g* tensors at the same level of theory and with the same basis set for all molecules. We have not considered zero-point vibrational corrections in this work.

All calculations employ Dunning's correlation-consistent basis sets.[61,62] Since it has previously been noted that diffuse functions are important in calculating magnetizabilities and rotational *g* tensors,[5,14,49] the augmented correlation-consistent double- and triple-ζ basis sets aug-cc-pVDZ and aug-cc-pVTZ were used, with some additional calculations carried out in the corresponding quadruple-ζ aug-cc-pVQZ basis to assess basis-set convergence.

In this work, we have calculated the mean relative deviations, mean absolute deviations, and standard deviations as

$$\bar{\Delta} = \frac{1}{n}\sum_{i=1}^{n}\Delta_i \tag{14}$$

$$\bar{\Delta}_{abs} = \frac{1}{n}\sum_{i=1}^{n}|\Delta_i| \tag{15}$$

$$\Delta_{std} = \sqrt{\frac{1}{n-1}\sum_{i=1}^{n}(\Delta_i - \bar{\Delta})^2} \tag{16}$$

where the summations are over the *n* individual errors in the calculated tensor elements of all molecules

$$\Delta_i = g_i^{calc} - g_i^{ref} \tag{17}$$

Since the rotational *g* tensor elements differ widely in magnitude, we have also calculated the percentage mean absolute deviations

$$\bar{\Delta}_{pabs} = \frac{100}{n}\sum_{i=1}^{n}\left|\frac{g_i^{calc} - g_i^{ref}}{g_i^{ref}}\right| \tag{18}$$

as an alternative to the mean absolute deviations, eq 15.

IV. Comparison with Experiment

A. Experimental Data. With four exceptions, all experimental gas-phase rotational *g* tensors listed here have been reported by Flygare and co-workers.[2,3] These measurements, which were carried out in the 1960s and early 1970s, still represent the standard compilation of experimental gas-phase rotational *g* tensors. More recent experimental data were included only where they are more accurate than those of Flygare, as defined by smaller error bars and a greater number of significant figures. The four exceptions are OCS, ClCN, O_3, and SO_2, which all arise from the work of Dymanus and co-workers.[63−66]

For OCS, the data of ref 63 is included, since three isotopes are studied whereas Flygare only reported two. The magnitude of the experimental *g* tensors and associated error bars is consistent for the two isotopes reported in both references.

Table 3. Linear Regression Results from a Comparison of Calculated and Experimental Data[a]

	optimized geometry		exptl geometry		optimized geometry		exptl geometry	
method	DZ	TZ	DZ	TZ	DZ	TZ	DZ	TZ
	R^2 Values				Slope of Linear Equation			
HF	0.936	0.941	0.862	0.866	0.97	0.96	0.83	0.84
LDA	0.930	0.997	0.992	0.999	1.10	0.89	0.87	0.88
BLYP	0.940	0.995	0.999	0.999	1.21	0.93	0.95	0.95
B3LYP	0.950	0.990	0.994	0.994	1.30	0.94	0.95	0.95
KT1	0.931	0.998	0.999	0.999	1.28	0.99	0.99	1.00
KT2	0.909	0.998	0.999	0.999	1.24	1.00	1.01	1.02
KT3	0.883	0.997	0.999	0.999	1.18	1.00	1.02	1.03

[a] Linear regression is forced to pass through the origin with the experimental data on the *y* axis.

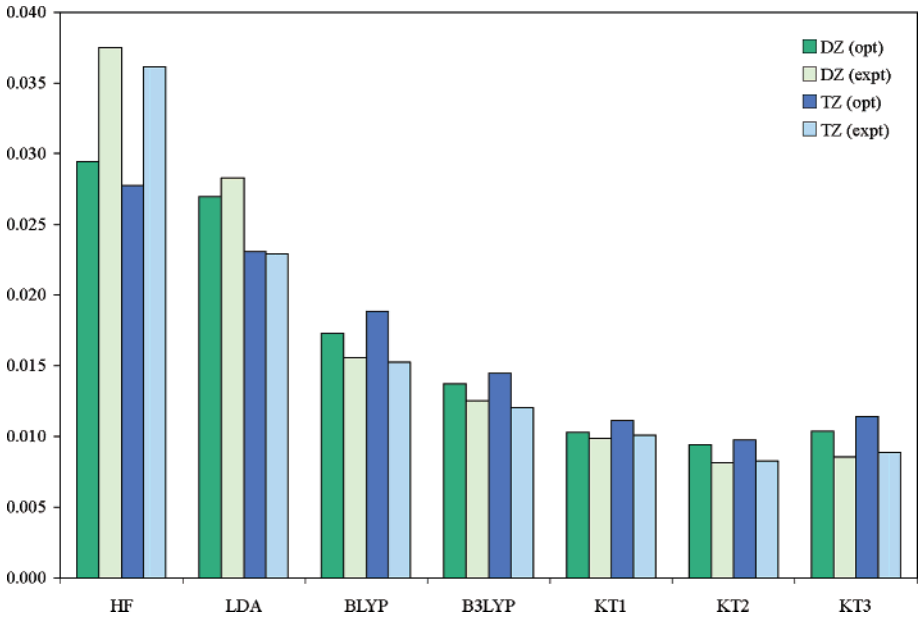

Figure 1. Mean absolute deviation from experimental *g* tensors for Hartree−Fock and DFT methods at both optimized and experimental geometries.

Dynamus' data[65] for O_3 (−2.9877 ± 0.0009, −0.2295 ± 0.0003, −0.0760 ± 0.0003) is used rather than Flygare's (−2.968 ± 0.035, −0.228 ± 0.007, −0.081 ± 0.006) and similarly for SO_2.[64] The ClCN *g* tensor of Reinartz and co-workers[66] (−0.041 21 ± 0.000 13) supersedes the value of Flygare (−0.0384 ± 0.0003).

B. Statistical Analysis. In Table 2, we summarize the calculated rotational *g* tensor elements as deviations from the highly accurate experimental data, and in Table 3, we present data from a linear regression analysis. These results are further illustrated in Figure 1, where $\bar{\Delta}_{abs}$ is plotted for each respective method. The DFT results are clearly superior to the Hartree−Fock results, which is in agreement with that of Wilson and co-workers,[48] who considered a small sample size of seven molecules without the use of London orbitals.

Of the functionals considered, the results in Figure 1 and Table 2 indicate that the KT functionals perform better than the standard SVWN, BLYP, and B3LYP functionals, with the KT2 functional being the best functional of those considered in this work. This observation gives further confirmation of the superior performance of KT functionals for properties involving an external magnetic field.[58] In contrast to the Hartree−Fock calculations, the DFT calculations at the experimental geometry typically produce rotational *g* tensors that are closer to experimental results than those obtained at the optimized geometries.

As in a previous study of the magnetizability of hydrocarbons,[67] we have carried out a linear regression analysis to examine the relationship between the calculated and experimental data. Our results are collected in Table 3, where the superior performance of DFT relative to Hartree−Fock theory is clearly demonstrated, both in terms of the slope of the fitted linear equation and the R^2 values. In particular, the slope of 1.00 ± 0.03 for the KT functionals highlights the ability of these functionals to reproduce experimental results—see Figure 2, where the KT2/aug-cc-pVTZ results (at the experimental geometries) are plotted against the experimental data. Even for the outliers, this functional accurately reproduces experimental results.

From Table 2, we see that basis-set effects are small for rotational *g* tensors calculated with London orbitals. Indeed, it has been shown previously that Hartree−Fock magnetizabilities and *g* tensors converge rapidly with London orbitals, with reasonably accurate results often obtained in the aug-cc-pVDZ basis.[5,44] To test the basis-set convergence, additional aug-cc-pVQZ calculations were performed for the *g* tensors of the linear molecules in Table 1, giving average and maximum differences between the aug-cc-pVTZ and aug-cc-pVQZ basis sets of 0.0002 and 0.0014, respectively.

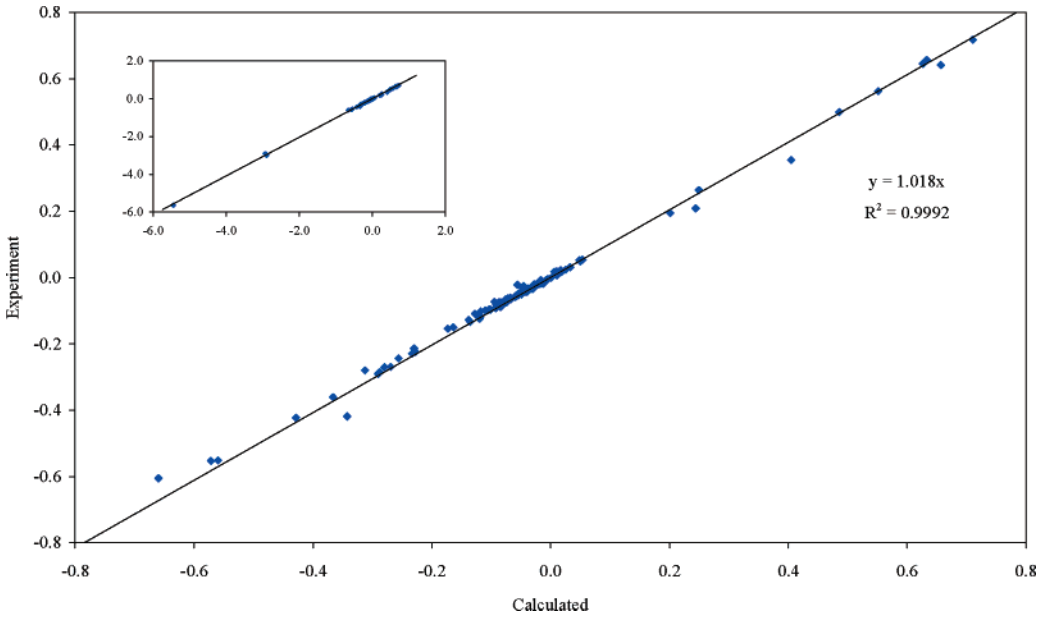

Figure 2. Correlation between KT2/aug-cc-pVTZ calculated and experimental rotational *g* tensors, with all calculations performed at experimental geometries. The inset includes the entire data range of included *g* tensor elements.

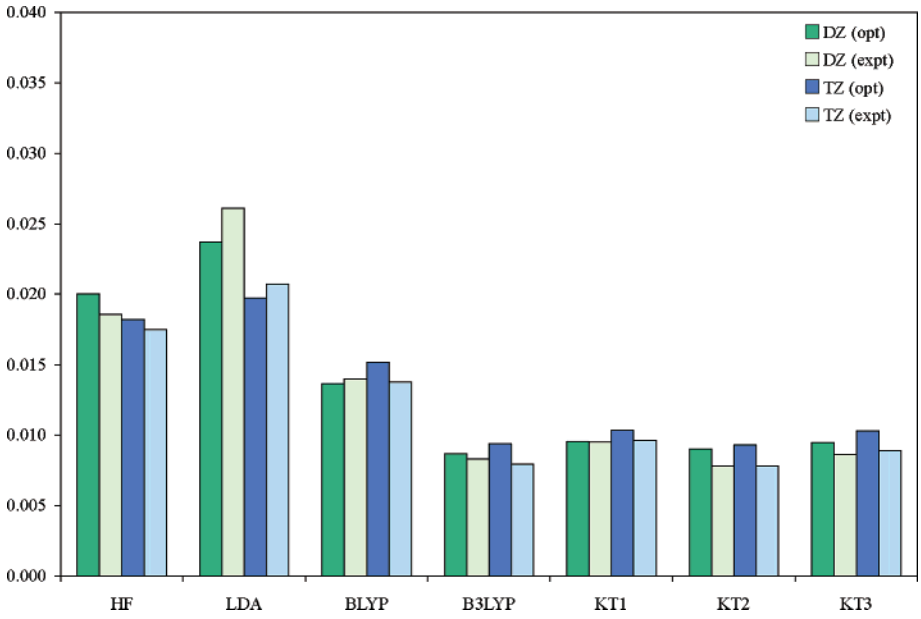

Figure 3. Mean absolute deviation from experimental *g* tensors for Hartree−Fock and DFT methods at both optimized and experimental geometries, excluding ozone.

The average and maximum differences between the aug-cc-pVDZ and aug-cc-pVTZ basis sets are 0.0015 and 0.0044, respectively. This observation is true for all methods (Hartree−Fock as well as DFT) considered here.

C. Ozone. Of the molecules included in our sample, ozone may be considered a special case, representing a system with large static and dynamic correlation corrections for which, in wave function theory, a multiconfigurational treatment is mandatory. Moreover, its rotational *g* tensor is particularly sensitive to changes in the geometry.[49] We note that the magnitude of the largest component of the *g* tensor is very large compared to the average range of values—see Figure 2, where the experimental principal g_{xx} element of O_3 lies well outside the typical range of values. For these reasons, we have listed the ozone *g* tensor elements separately in Table 4.

The poor performance of the Hartree−Fock method for the *g* tensor of ozone is obvious, with a fortuitous cancellation of errors that gives results closer to experimental results at the optimized geometry than at the experimental geometry (as is typical of all Hartree−Fock calculations). The geometry dependence of the rotational *g* tensor for ozone is also noticeable for DFT, with the difference in *g* tensor elements between the optimized and experimental geometries typically several orders of magnitude larger than the experimental standard deviations. Again, we note the superior performance of the KT functionals, even for the difficult ozone system.

To compare with experimental results and to understand the differences in geometry with calculated properties, it is often important to consider zero-point vibrational effects at optimized geometries. In a previous MCSCF study of ozone,

Table 4. Calculated Rotational *g* Tensors of Ozone (aug-cc-pVTZ Basis)

method	g_{xx}	g_{yy}	g_{zz}
	Optimized Geometry		
HF	−4.4843	−0.2578	−0.0681
LDA	−3.5619	−0.2285	−0.0787
BLYP	−3.5878	−0.2398	−0.0811
B3LYP	−3.7853	−0.2460	−0.0767
KT1	−3.1310	−0.2295	−0.0799
KT2	−3.0752	−0.2238	−0.0782
KT3	−3.1809	−0.2233	−0.0773
	Experimental Geometry		
HF	−5.7515	−0.3992	−0.0675
LDA	−3.3687	−0.2473	−0.0808
BLYP	−3.2387	−0.2460	−0.0826
B3LYP	−3.6049	−0.2677	−0.0786
KT1	−2.8966	−0.2335	−0.0812
KT2	−2.9021	−0.2334	−0.0797
KT3	−2.9748	−0.2355	−0.0791
exptl	−2.9877(9)	−0.2295(3)	−0.0760(3)

the zero-point vibrational corrections were found to be −0.0707 (g_{xx}), −0.0018 (g_{yy}), and −0.0014 (g_{zz}).[49] For the principal g_{xx} component, therefore, the inclusion of vibrational corrections worsens the agreement with experiment, for all methods. Moreover, for the g_{zz} component, only the Hartree−Fock result is closer to experimental results with the inclusion of vibrational corrections, whereas for the g_{yy} component, only the KT2 and KT3 functional results are closer to experimental results.

Since ozone is such a difficult special case, we have repeated the statistical analysis with ozone excluded from the sample set. Comparing Figures 1 and 3, we see that the exclusion of ozone markedly reduces the Hartree−Fock deviations from experimental results. Also, with the exclusion of ozone, the B3LYP performance improves markedly relative to that of the KT2 functional. Thus, with the exception of the KT functionals, ozone has a very clear and disproportionate effect on the total calculated statistics.

Table 5. Calculated *g* Tensors at Optimized Geometries, Linear Molecules

method	experiment	HF	LDA	BLYP	B3LYP	KT1	KT2	KT3
CO	−0.2689 ± 0.0001	−0.2736	−0.2864	−0.2832	−0.2811	−0.2723	−0.2698	−0.2744
CS	−0.2702 ± 0.0004	−0.2921	−0.3026	−0.2912	−0.2926	−0.2814	−0.2794	−0.2819
CSe	−0.2431 ± 0.0016	−0.2919	−0.2758	−0.2666	−0.2734	−0.2565	−0.2553	−0.2562
$HC^{15}N$	−0.0904 ± 0.0003	−0.0721	−0.1042	−0.1034	−0.0963	−0.0955	−0.0937	−0.0975
$FC^{15}N$	−0.0504 ± 0.0008	−0.0497	−0.0530	−0.0518	−0.0518	−0.0480	−0.0484	−0.0487
$ClC^{15}N$	−0.04121 ± 0.000 13	−0.0365	−0.0422	−0.0415	−0.0404	−0.0403	−0.0403	−0.0406
$BrC^{15}N$	−0.0325 ± 0.0010	−0.0315	−0.0354	−0.0350	−0.0342	−0.0342	−0.0342	−0.0344
OCS	−0.0288 39 ± 0.000 006	−0.0271	−0.0304	−0.0313	−0.0301	−0.0296	−0.0294	−0.0297
$OC^{34}S$	−0.0282 42 ± 0.000 010	−0.0265	−0.0298	−0.0306	−0.0295	−0.0290	−0.0288	−0.0291
$O^{13}CS$	−0.0287 10 ± 0.000 015	−0.0270	−0.0303	−0.0311	−0.0300	−0.0295	−0.0293	−0.0296
^{15}NNO	−0.076 06 ± 0.000 10	−0.0768	−0.0802	−0.0807	−0.0801	−0.0781	−0.0779	−0.0784
^{14}NNO	−0.078 87 ± 0.000 08	−0.0793	−0.0831	−0.0835	−0.0829	−0.0809	−0.0806	−0.0811
$OC^{80}Se$	−0.019 52 ± 0.000 10	−0.0176	−0.0212	−0.0219	−0.0209	−0.0206	−0.0204	−0.0208
$OC^{76}Se$	−0.019 69 ± 0.000 10	−0.0178	−0.0214	−0.0221	−0.0211	−0.0208	−0.0206	−0.0210
HCP	−0.0430 ± 0.0010	−0.0311	−0.0532	−0.0507	−0.0471	−0.0446	−0.0439	−0.0454
DCP	−0.0353 ± 0.0010	−0.0266	−0.0454	−0.0434	−0.0402	−0.0382	−0.0376	−0.0389
HBS	−0.0414 ± 0.0002	−0.0288	−0.0496	−0.0472	−0.0433	−0.0427	−0.0414	−0.0414
FCCH	−0.0077 ± 0.0002	−0.0050	−0.0098	−0.0106	−0.0093	−0.0077	−0.0078	−0.0084
$^{35}ClCCH$	−0.006 30 ± 0.000 14	−0.0029	−0.0089	−0.0090	−0.0075	−0.0077	−0.0077	−0.0079
$^{37}ClCCH$	−0.006 01 ± 0.000 08	−0.0027	−0.0087	−0.0088	−0.0073	−0.0075	−0.0075	−0.0077
$^{79}BrCCH$	−0.003 95 ± 0.000 32	−0.0017	−0.0066	−0.0070	−0.0057	−0.0061	−0.0061	−0.0063
$^{81}BrCCH$	−0.003 88 ± 0.000 14	−0.0016	−0.0065	−0.0070	−0.0056	−0.0061	−0.0060	−0.0063

Table 6. Calculated *g* Tensors at Optimized Geometries, Symmetric Tops

method	experiment	HF	LDA	BLYP	B3LYP	KT1	KT2	KT3
$^{15}NH_3$	0.563 ± 0.002	0.5906	0.5870	0.5427	0.5626	0.5416	0.5488	0.5386
	0.500 ± 0.002	0.5083	0.5195	0.4780	0.4914	0.4846	0.4879	0.4791
CHF_3	−0.0359 ± 0.0008	−0.0349	−0.0392	−0.0388	−0.0377	−0.0382	−0.0380	−0.0379
	−0.031[a]	−0.0329	−0.0345	−0.0347	−0.0342	−0.0340	−0.0339	−0.0336
$CH_3{}^{14}NC$	−0.0546 ± 0.0015	−0.0548	−0.0643	−0.0631	−0.0612	−0.0611	−0.0607	−0.0614
	0.31[a]	0.2990	0.3275	0.2782	0.2917	0.2862	0.2893	0.2776
$CH_3C^{15}N$	−0.0317 ± 0.0003	−0.0283	−0.0352	−0.0370	−0.0346	−0.0353	−0.0346	−0.0355
	0.31[a]	0.3315	0.3590	0.3056	0.3209	0.3163	0.3198	0.3082
$CH_3C^{14}N$	−0.0338 ± 0.0008	−0.0302	−0.0373	−0.0391	−0.0366	−0.0373	−0.0367	−0.0376
	0.31[a]	0.3315	0.3590	0.3056	0.3209	0.3163	0.3198	0.3082
$CD_3C^{14}N$	−0.0315 ± 0.0008	−0.0290	−0.0349	−0.0364	−0.0343	−0.0348	−0.0343	−0.0351
	0.31[a]	0.1659	0.1797	0.1529	0.1606	0.1583	0.1600	0.1542
CH_3F	−0.062 ± 0.002	−0.0589	−0.0715	−0.0682	−0.0655	−0.0687	−0.0681	−0.0678
	0.265 ± 0.008	0.2654	0.2793	0.2415	0.2555	0.2457	0.2485	0.2374
CH_3Cl	−0.0165 ± 0.003	−0.0095	−0.0202	−0.0193	−0.0166	−0.0196	−0.0192	−0.0189
	0.305[a]	0.2959	0.3095	0.2709	0.2835	0.2744	0.2765	0.2664

[a] Assumed value.

Table 7. Calculated *g* Tensors at Optimized Geometries, Nonring Planar Asymmetric Tops

method	experiment	HF	LDA	BLYP	B3LYP	KT1	KT2	KT3
methyl butadiene	−0.0621 ± 0.0013	−0.0569	−0.0726	−0.0712	−0.0679	−0.0690	−0.0684	−0.0679
C_5H_8	−0.0339 ± 0.0016	−0.0315	−0.0368	−0.0359	−0.0349	−0.0355	−0.0351	−0.0345
	0.0080 ± 0.0016	0.0118	0.0121	0.0078	0.0094	0.0098	0.0101	0.0090
acrolein	−0.5512 ± 0.0019	−0.5019	−0.6409	−0.6171	−0.5917	−0.5874	−0.5820	−0.5842
C_3H_4O	−0.0567 ± 0.0010	−0.0571	−0.0618	−0.0601	−0.0598	−0.0590	−0.0587	−0.0583
	−0.0080 ± 0.0010	−0.0057	−0.0077	−0.0098	−0.0084	−0.0085	−0.0084	−0.0085
propene	−0.0789 ± 0.0006	−0.0660	−0.0981	−0.1063	−0.0953	−0.0960	−0.0949	−0.0983
C_3H_6	−0.0424 ± 0.0004	−0.0401	−0.0468	−0.0470	−0.0452	−0.0466	−0.0459	−0.0456
	0.0107 ± 0.0005	0.0150	0.0120	0.0075	0.0101	0.0088	0.0095	0.0092
propynal	−0.553 ± 0.002	−0.5135	−0.6525	−0.6184	−0.5970	−0.5876	−0.5836	−0.5880
C_3H_2O	−0.040 ± 0.002	−0.0359	−0.0458	−0.0440	−0.0426	−0.0412	−0.0409	−0.0408
	−0.015 ± 0.001	−0.0110	−0.0165	−0.0168	−0.0155	−0.0149	−0.0148	−0.0151
methoxy methane	−0.0214 ± 0.0006	−0.0036	−0.0441	−0.0437	−0.0309	−0.0505	−0.0482	−0.0425
CH_3OCH_3	−0.0093 ± 0.0004	−0.0053	−0.0089	−0.0118	−0.0095	−0.0115	−0.0110	−0.0115
	−0.0210 ± 0.0006	−0.0190	−0.0230	−0.0256	−0.0234	−0.0254	−0.0250	−0.0250
dimethyl sulfane	−0.0193 ± 0.0007	−0.0089	−0.0307	−0.0284	−0.0224	−0.0332	−0.0324	−0.0291
CH_3SCH_3	0.0000 ± 0.0003	0.0052	0.0017	−0.0023	0.0003	−0.0008	−0.0004	−0.0006
	−0.0083 ± 0.0003	−0.0050	−0.0075	−0.0105	−0.0087	−0.0084	−0.0083	−0.0087
acetaldehyde	−0.3609 ± 0.0021	−0.3306	−0.3999	−0.3977	−0.3836	−0.3711	−0.3660	−0.3670
C_2H_4O	−0.0731 ± 0.0003	−0.0718	−0.0783	−0.0782	−0.0770	−0.0762	−0.0752	−0.0755
	−0.0245 ± 0.0006	−0.0222	−0.0251	−0.0278	−0.0259	−0.0249	−0.0243	−0.0247
formaldehyde	−2.9017 ± 0.0008	−2.6654	−3.2558	−3.0868	−3.0179	−2.9677	−2.9331	−2.9174
H_2CO	−0.2243 ± 0.0001	−0.2190	−0.2390	−0.2363	−0.2329	−0.2316	−0.2286	−0.2293
	−0.0994 ± 0.0001	−0.0827	−0.1196	−0.1149	−0.1057	−0.1102	−0.1085	−0.1088
thioformaldehyde	−5.6202 ± 0.0068	−4.7503	−6.1903	−5.8301	−5.6519	−5.5662	−5.5358	−5.4496
H_2CS	−0.1337 ± 0.0004	−0.1335	−0.1452	−0.1412	−0.1403	−0.1371	−0.1354	−0.1352
	−0.0239 ± 0.0004	−0.0108	−0.0292	−0.0294	−0.0241	−0.0286	−0.0274	−0.0265
formic acid	−0.0903 ± 0.0006	−0.0891	−0.0964	−0.0942	−0.0936	−0.0926	−0.0922	−0.0914
HCOOH	−0.2797 ± 0.0060	−0.2511	−0.3002	−0.3003	−0.2913	−0.2840	−0.2811	−0.2877
	−0.0270 ± 0.0006	−0.0267	−0.0271	−0.0290	−0.0282	−0.0280	−0.0278	−0.0281
formamide	−0.0649 ± 0.0004	−0.0627	−0.0685	−0.0686	−0.0675	−0.0671	−0.0665	−0.0662
$HCONH_2$	−0.2843 ± 0.0011	−0.2530	−0.3186	−0.3175	−0.3050	−0.2969	−0.2948	−0.3002
	−0.0117 ± 0.0004	−0.0091	−0.0104	−0.0130	−0.0117	−0.0117	−0.0115	−0.0119
glycoaldehyde	−0.0726 ± 0.0010	−0.0389	−0.0428	−0.0421	−0.0414	−0.0416	−0.0412	−0.0411
$C_2H_4O_2$	−0.1239 ± 0.0013	−0.3136	−0.3990	−0.3754	−0.3644	−0.3621	−0.3589	−0.3575
	−0.0178 ± 0.0010	−0.0198	−0.0231	−0.0234	−0.0223	−0.0228	−0.0227	−0.0225
methyl formate	−0.0391 ± 0.0009	−0.0350	−0.0384	−0.0376	−0.0372	−0.0373	−0.0371	−0.0370
$C_2H_4O_2$	−0.1267 ± 0.0010	−0.2244	−0.2662	−0.2707	−0.2608	−0.2577	−0.2556	−0.2581
	−0.0168 ± 0.0017	−0.0200	−0.0214	−0.0218	−0.0213	−0.0212	−0.0212	−0.0213
ketene	−0.4182 ± 0.0009	−0.3208	−0.2931	−0.4391	−0.4030	−0.3812	−0.3715	−0.4015
$C_2H_2O_2$	−0.0356 ± 0.0013	−0.0349	−0.0363	−0.0383	−0.0372	−0.0359	−0.0354	−0.0361
	−0.0238 ± 0.0006	−0.0243	−0.0241	−0.0284	−0.0269	−0.0262	−0.0256	−0.0266
difluoro methane	−0.0411 ± 0.0004	−0.0407	−0.0441	−0.0427	−0.0421	−0.0422	−0.0421	−0.0419
CH_2F_2	−0.0725 ± 0.0006	−0.0589	−0.0963	−0.0872	−0.0789	−0.0906	−0.0894	−0.0891
	−0.0398 ± 0.0004	−0.0389	−0.0420	−0.0425	−0.0414	−0.0421	−0.0418	−0.0416
carbonic difluoride	−0.0568 ± 0.0006	−0.0538	−0.0618	−0.0604	−0.0594	−0.0586	−0.0585	−0.0582
F_2CO	−0.0747 ± 0.0004	−0.0756	−0.0799	−0.0777	−0.0778	−0.0749	−0.0750	−0.0751
	−0.0328 ± 0.0006	−0.0327	−0.0336	−0.0338	−0.0334	−0.0329	−0.0330	−0.0328
formyl fluoride	−0.4227 ± 0.0007	−0.4108	−0.4719	−0.4550	−0.4495	−0.4417	−0.4389	−0.4422
HFCO	−0.0771 ± 0.0002	−0.0777	−0.0822	−0.0805	−0.0804	−0.0787	−0.0785	−0.0782
	−0.0371 ± 0.0002	−0.0373	−0.0390	−0.0398	−0.0390	−0.0387	−0.0386	−0.0387
fluoro ethene	−0.1533 ± 0.0008	−0.1392	−0.1872	−0.1839	−0.1735	−0.1732	−0.1726	−0.1769
C_2H_3F	−0.0526 ± 0.0001	−0.0526	−0.0575	−0.0568	−0.0560	−0.0554	−0.0551	−0.0551
	−0.0037 ± 0.0001	−0.0011	−0.0034	−0.0066	−0.0047	−0.0055	−0.0051	−0.0055
1,1-difluoro ethene	−0.0421 ± 0.0005	−0.0407	−0.0453	−0.0470	−0.0455	−0.0446	−0.0446	−0.0450
CH_2CF_2	−0.0466 ± 0.0004	−0.0482	−0.0548	−0.0527	−0.0518	−0.0508	−0.0507	−0.0508
	−0.0119 ± 0.0004	−0.0107	−0.0121	−0.0140	−0.0128	−0.0132	−0.0130	−0.0131
cis-difluoro ethene	−0.1015 ± 0.0009	−0.0999	−0.1180	−0.1167	−0.1121	−0.1162	−0.1154	−0.1153
CHFCHF	−0.0296 ± 0.0003	−0.0292	−0.0332	−0.0324	−0.0318	−0.0309	−0.0308	−0.0308
	−0.0158 ± 0.0002	−0.0151	−0.0169	−0.0174	−0.0167	−0.0167	−0.0166	−0.0168
fluoro ethane	0.0185 ± 0.0006	0.0278	0.0119	0.0071	0.0147	0.0056	0.0075	0.0077
C_2H_5F	−0.0124 ± 0.0003	−0.0095	−0.0118	−0.0144	−0.0125	−0.0135	−0.0130	−0.0133
	−0.0197 ± 0.0004	−0.0196	−0.0213	−0.0239	−0.0222	−0.0230	−0.0226	−0.0227
trifluoro ethene	−0.0503 ± 0.0002	−0.0494	−0.0578	−0.0570	−0.0550	−0.0555	−0.0553	−0.0554
C_2HF_2	−0.0321 ± 0.0002	−0.0331	−0.0349	−0.0344	−0.0341	−0.0336	−0.0335	−0.0333
	−0.0170 ± 0.0002	−0.0172	−0.0173	−0.0180	−0.0177	−0.0173	−0.0173	−0.0174
ozone	−2.9877 ± 0.0009	−4.4843	−3.5619	−3.5878	−3.7853	−3.1310	−3.0752	−3.1809

Table 7. Continued

method	experiment	HF	LDA	BLYP	B3LYP	KT1	KT2	KT3
O_3	−0.2295 ± 0.0003	−0.2578	−0.2285	−0.2398	−0.2460	−0.2295	−0.2238	−0.2233
	−0.0760 ± 0.0003	−0.0681	−0.0787	−0.0811	−0.0767	−0.0799	−0.0782	−0.0773
sulfur dioxide	−0.6043 ± 0.0003	−0.6257	−0.6833	−0.7029	−0.6848	−0.6819	−0.6664	−0.6767
SO_2	−0.116 34 ± 0.000 12	−0.1159	−0.1242	−0.1260	−0.1240	−0.1234	−0.1221	−0.1220
	−0.088 65 ± 0.000 10	−0.0889	−0.0839	−0.0830	−0.0846	−0.0816	−0.0821	−0.0818
difluoro oxide	−0.213 ± 0.005	−0.1335	−0.2561	−0.2873	−0.2218	−0.2438	−0.2324	−0.2408
OF_2	−0.058 ± 0.002	−0.0444	−0.0634	−0.0679	−0.0594	−0.0618	−0.0600	−0.0605
	−0.068 ± 0.002	−0.0583	−0.0742	−0.0787	−0.0728	−0.0739	−0.0722	−0.0721
hypofluoros acid	0.642 ± 0.001	0.7050	0.6680	0.6430	0.6641	0.6407	0.6496	0.6450
HOF	−0.119 ± 0.001	−0.0856	−0.1239	−0.1349	−0.1184	−0.1223	−0.1182	−0.1205
	−0.061 ± 0.001	−0.0460	−0.0733	−0.0769	−0.0675	−0.0706	−0.0686	−0.0701
water	0.718 ± 0.007	0.7468	0.7309	0.7001	0.7168	0.6984	0.7051	0.6982
H_2O	0.657 ± 0.001	0.6911	0.6591	0.6271	0.6497	0.6250	0.6356	0.6326
	0.645 ± 0.006	0.6684	0.6534	0.6206	0.6376	0.6212	0.6268	0.6200
hydrogen sulfide	0.355 ± 0.008	0.3893	0.4286	0.3692	0.3844	0.4008	0.4030	0.3907
H_2S	0.195 ± 0.008	0.1767	0.2419	0.1586	0.1756	0.1945	0.1942	0.1747
	0.209 ± 0.008	0.1966	0.2858	0.2151	0.2211	0.2488	0.2467	0.2299

Table 8. Calculated *g* Tensors at Optimized Geometries, Three-Member Rings

method	experiment	HF	LDA	BLYP	B3LYP	KT1	KT2	KT3
methylenecyclopropane	−0.0672 ± 0.0007	−0.0542	−0.0769	−0.0805	−0.0734	−0.0772	−0.0761	−0.0769
C_4H_6	−0.0231 ± 0.0004	−0.0193	−0.0258	−0.0277	−0.0253	−0.0256	−0.0250	−0.0257
	0.0244 ± 0.0004	0.0306	0.0267	0.0227	0.0254	0.0239	0.0245	0.0240
cyclopropene	−0.0897 ± 0.0009	−0.0918	−0.0981	−0.1010	−0.0977	−0.0941	−0.0927	−0.0958
C_3H_4	−0.1492 ± 0.0002	−0.1479	−0.1665	−0.1623	−0.1590	−0.1630	−0.1621	−0.1610
	0.0536 ± 0.0002	0.0629	0.0529	0.0477	0.0527	0.0479	0.0488	0.0473
aziridine	0.0229 ± 0.0009	0.0379	0.0206	0.0157	0.0224	0.0193	0.0204	0.0198
C_2H_5N	−0.0422 ± 0.0008	−0.0254	−0.0503	−0.0505	−0.0433	−0.0460	−0.0453	−0.0453
	0.0539 ± 0.0010	0.0613	0.0550	0.0478	0.0524	0.0525	0.0531	0.0510
oxirane	0.0189 ± 0.0004	0.0329	0.0139	0.0090	0.0164	0.0107	0.0123	0.0113
C_2H_4O	−0.0946 ± 0.0003	−0.0889	−0.1094	−0.1065	−0.1012	−0.1010	−0.1009	−0.1020
	0.0318 ± 0.0006	0.0381	0.0341	0.0277	0.0317	0.0325	0.0328	0.0309
thiirane	−0.0159 ± 0.0021	0.0033	−0.0187	−0.0240	−0.0159	−0.0186	−0.0177	−0.0182
C_2H_4S	−0.0242 ± 0.0003	−0.0149	−0.0302	−0.0308	−0.0262	−0.0300	−0.0294	−0.0291
	0.0487 ± 0.0004	0.0551	0.0501	0.0454	0.0486	0.0493	0.0496	0.0479
cyclopropenone	−0.2900 ± 0.0013	−0.2615	−0.3186	−0.3101	−0.3002	−0.2988	−0.2956	−0.2955
C_3H_2O	−0.0963 ± 0.0004	−0.0938	−0.1058	−0.1035	−0.1014	−0.1005	−0.0999	−0.0997
	−0.0121 ± 0.0004	−0.0062	−0.0128	−0.0154	−0.0124	−0.0165	−0.0161	−0.0157
methyl cyclopropene	−0.0813 ± 0.0070	−0.0816	−0.0927	−0.0968	−0.0734	−0.0951	−0.0940	−0.0954
C_4H_6	−0.0261 ± 0.0040	−0.0276	−0.0296	−0.0320	−0.0253	−0.0312	−0.0307	−0.0309
	0.0166 ± 0.0030	0.0220	0.0188	0.0152	0.0254	0.0155	0.0161	0.0156

D. Comments on Other Specific Molecules. The accuracy and applicability of DFT *g* tensors may further be illustrated by examining some specific cases. In Tables 5−9, we present individual *g* tensors calculated at optimized geometries with the aug-cc-pVTZ basis set.

As discussed above, the two experimental values reported for ClCN are those of Reinartz et al.[66] (−0.041 21 ± 0.000 13) and Flygare (−0.0384 ± 0.0003). Our London DFT results support the more recent value of Reinartz et al., although vibrational corrections are needed for a more definite assessment.

Next, comparing the *g* values of CO, CS, and CSe in Table 5, we note that the GGA and hybrid DFT results are sufficiently accurate to distinguish properly among these analogues, giving the correct ordering $|g_{CSe}| < |g_{CO}| < |g_{CS}|$. By contrast, the Hartree−Fock and LDA models mix CO and CSe, giving instead $|g_{CSe}| < |g_{CS}| < |g_{CO}|$. Again, the best results are provided by the KT2 functional, with all other methods giving *g* values that are too large in magnitude.

The halogenated cyanides HCN, FCN, ClCN, and BrCN may be readily distinguished from their calculated rotational *g* tensors, in agreement with experimental results. By contrast, at the optimized geometries, the results for the halogenated acetylenes FCCH, ClCCH, and BrCCH do not reproduce the experimental trends accurately, except for the usually unreliable Hartree−Fock model (which gets trends right but severely underestimates the *g* values). However, this situation changes when the calculations are carried out at experimental rather than optimized geometries: the Hartree−Fock model then no longer works, but all DFT functionals distinguish correctly between the three species.

In the experimental studies of the CH_3CN isotopes and isomers, the parallel *g* component was given an assumed value of 0.310. Our calculations indicate that this assumption

Table 9. Calculated *g* Tensors at Optimized Geometries, Four-Member Rings

method	experiment	HF	LDA	BLYP	B3LYP	KT1	KT2	KT3
cyclobutene	−0.0516 ± 0.0007	−0.0496	−0.0596	−0.0604	−0.0574	−0.0580	−0.0571	−0.0578
C_4H_6	−0.0663 ± 0.0007	−0.0614	−0.0771	−0.0777	−0.0734	−0.0773	−0.0765	−0.0758
	−0.0219 ± 0.0006	−0.0146	−0.0180	−0.0243	−0.0207	−0.0270	−0.0257	−0.0256
oxetane	−0.0073 ± 0.0005	0.0013	−0.0127	−0.0146	−0.0094	−0.0146	−0.0131	−0.0135
C_3H_6O	−0.0429 ± 0.0007	−0.0357	−0.0497	−0.0501	−0.0455	−0.0491	−0.0481	−0.0482
	−0.0747 ± 0.0005	−0.0683	−0.0806	−0.0799	−0.0768	−0.0847	−0.0832	−0.0813
methylenecyclobutane	−0.0320 ± 0.0008	−0.0243	−0.0364	−0.0420	−0.0368	−0.0381	−0.0372	−0.0385
C_5H_8	−0.0218 ± 0.0010	−0.0196	−0.0241	−0.0258	−0.0239	−0.0241	−0.0235	−0.0240
	−0.0184 ± 0.0011	−0.0132	−0.0151	−0.0193	−0.0172	−0.0185	−0.0177	−0.0180
cyclobutanone	−0.0740 ± 0.0020	−0.0737	−0.0953	−0.0951	−0.0903	−0.0891	−0.0876	−0.0887
C_4H_6O	−0.0325 ± 0.0004	−0.0329	−0.0358	−0.0375	−0.0361	−0.0359	−0.0353	−0.0356
	−0.0279 ± 0.0004	−0.0270	−0.0271	−0.0296	−0.0287	−0.0290	−0.0285	−0.0285
β-propiolactone	−0.0758 ± 0.0005	−0.0708	−0.0862	−0.0893	−0.0845	−0.0853	−0.0841	−0.0850
$C_3H_4O_2$	−0.0356 ± 0.0004	−0.0355	−0.0396	−0.0398	−0.0386	−0.0391	−0.0387	−0.0389
	−0.0319 ± 0.0004	−0.0317	−0.0315	−0.0334	−0.0327	−0.0332	−0.0328	−0.0328
diketene	−0.1091 ± 0.0004	−0.1000	−0.1226	−0.1246	−0.1185	−0.1193	−0.1180	−0.1188
$C_4H_4O_2$	−0.0324 ± 0.0004	−0.0337	−0.0359	−0.0357	−0.0351	−0.0348	−0.0346	−0.0348
	−0.0169 ± 0.0004	−0.0169	−0.0167	−0.0185	−0.0177	−0.0183	−0.0180	−0.0179

is valid for $CH_3{}^{14}NC$, $CH_3C^{14}N$, and $CH_3C^{15}N$ but not for $CD_3C^{14}N$. For all methods, the parallel component for $CD_3C^{14}N$ is $^1/_2$ that for $CH_3C^{14}N$, indicating that a more appropriate value for the parallel component of $CD_3C^{14}N$ is 0.16 ± 0.01. By contrast, our calculations support the assumptions made in the experimental studies of CHF_3 and CH_3Cl, with assumed parallel *g* values of −0.031 and 0.305, respectively.

Apart from ozone, the two statistical outliers are the principal *g* tensor components of H_2CO (−2.9017) and H_2CS (−5.6202). In both cases, the optimized geometries agree with experimental results and, thus, contribute little to the observed differences from experimental *g* tensors. We note the particularly poor performance of the Hartree−Fock and LDA methods for these systems.

For methoxy methane, and to a lesser extent for dimethyl sulfane, all methods poorly reproduce the experimental g_{xx} value. The inclusion of core functions in the augmented correlation-consistent polarized core-valence basis sets aug-cc-pCVDZ and aug-cc-pCVTZ for dimethyl sulfane consistently makes all tensor components more negative. Moreover, the convergence from the aug-cc-pVDZ to aug-cc-pVTZ basis sets similarly makes all tensor components more negative. In light of these results, we suggest that the experimental g_{xx} components of these two molecules may be too positive.

E. Geometry Dependence. It has been shown previously[49] that calculated rotational *g* tensors are sensitive to molecular geometry, necessitating the use of accurate molecular geometries. To illustrate this dependence, the significant deviations between the calculated *g* tensor elements of glycoaldehyde and methyl formate in Table 7 may be attributed to geometry effects, with tensor elements calculated at the experimental geometries typically within 0.005 of experimental results, in contrast to the deviations of greater than 0.2 for the principal *g*-tensor component of glycoaldehyde.

We have considered the geometry dependence of calculated rotational *g* tensors by employing both experimentally determined and theoretically calculated equilibrium molecular geometries; that is, we consider both the intrinsic error of the method and the error associated with an optimized geometry.

From an analysis of the calculated geometries, we noted a clear trend for the methods considered in this work in that going from a double-ζ to a triple-ζ basis, the calculated bond lengths generally increased while bond angles were diminished. From Figures 1 and 3, it would appear that the GGA and hydrid DFT methods considered give more accurate results with a double-ζ basis set than with a triple-ζ basis set for both optimized and experimental geometries. In contrast, for the Hartree−Fock and LDA methods, triple-ζ results are typically closer to experimental results than the double-ζ results. For the calculation of rotational *g* tensors from optimized geometries, all methods, Hartree−Fock and LDA in particular, benefit from a fortuitous cancellation of errors; that is, the intrinsic error of these methods is largely canceled by the error associated with longer optimized bond lengths.

For the GGA and hybrid DFT functionals, the smallest deviation from experimental *g* tensors was calculated at experimental geometries, reinforcing previous conclusions[49] that accurate geometries are necessary for accurate calculations of rotational *g* tensors.

V. Conclusions

We have carried out extensive benchmarking of a number of DFT functionals with respect to the calculation of rotational *g* tensors. The performance and reliability of the DFT approach has been shown to be superior to Hartree−Fock theory in the calculation of this property, with GGA functionals performing better than the LDA functional. The KT functionals show the widest applicability and reliability of the functionals considered in this work, giving good results also for the difficult ozone molecule.

With the use of London orbitals, basis-set convergence is rapid for both Hartree−Fock and DFT methods, with good

agreement with experimental results in the aug-cc-pVDZ basis, and near-basis set limit results obtained in an aug-cc-pVTZ basis.

Acknowledgment. This work has received support from the Norwegian Reseach Council through a Strategic University Program in Quantum Chemistry (Grant 154011/420). D.J.D.W. has been supported by the Norwegian Research Council through a postdoctoral fellowship (Grant 155137/432). We also acknowledge a grant of computer time from the Norwegian Supercomputing Program.

References

(1) Ramsey, N. F. *Molecular Beams*; Clarendon Press: Oxford, 2000.

(2) Flygare, W. H.; Benson, R. C. *Mol. Phys.* **1971**, *20*, 225.

(3) Flygare, W. H. *Chem. Rev.* **1974**, *74*, 653.

(4) Kelly, H. M.; Fowler, P. W. *Chem. Phys. Lett.* **1993**, *206*, 568.

(5) Gauss, J.; Ruud, K.; Helgaker, T. *J. Chem. Phys.* **1996**, *105*, 2804.

(6) Ruud, K.; Helgaker, T. *Chem. Phys. Lett.* **1997**, *264*, 17.

(7) Bishop, D. M.; Cybulski, S. M. *J. Chem. Phys.* **1993**, *98*, 8057.

(8) Cybulski, S. M.; Bishop, D. M. *J. Chem. Phys.* **1994**, *100*, 2019.

(9) Cybulski, S. M.; Bishop, D. M. *J. Chem. Phys.* **1996**, *106*, 4082.

(10) Sauer, S. P. A.; Špirko, V.; Oddershede, J. *Chem. Phys.* **1991**, *153*, 189.

(11) Sauer, S. P. A. *Chem. Phys. Lett.* **1998**, *297*, 475.

(12) Ogilvie, J. F.; Oddershede, J.; Sauer, S. P. A. *Adv. Chem. Phys.* **1998**, *111*, 475.

(13) Åstrand, P. O.; Mikkelsen, K. V.; Ruud, K.; Helgaker, T. *J. Phys. Chem.* **1996**, *100*, 19771.

(14) Ruud, K.; Helgaker, T.; Jørgensen, P. *J. Chem. Phys.* **1997**, *107*, 10599.

(15) Ruud, K.; Vaara, J.; Lounila, J.; Helgaker, T. *Chem. Phys. Lett.* **1998**, *297*, 467.

(16) Ruud, K.; Åstrand, P. O.; Helgaker, T.; Mikkelsen, K. V. *THEOCHEM* **1996**, *388*, 231.

(17) Åstrand, P. O.; Ruud, K.; Mikkelsen, K. V.; Helgaker, T. *Chem. Phys. Lett.* **1997**, *271*, 163.

(18) Vosko, S. H.; Wilk, L.; Nusair, M. *Can. J. Phys.* **1980**, *58*, 1200.

(19) Becke, A. D. *Phys. Rev. A* **1988**, *38*, 3098.

(20) Miehlich, B.; Savin, A.; Stoll, H.; Preuss, H. *Chem. Phys. Lett.* **1989**, *157*, 200.

(21) Becke, A. D. *J. Chem. Phys.* **1993**, *98*, 5648.

(22) Becke, A. D. *Phys. Rev. A* **1988**, *38*, 3098.

(23) Lee, C.; Yang, W.; Parr, R. G. *Phys. Rev. B* **1988**, *37*, 785.

(24) Møller, C.; Plesset, M. S. *Phys. Rev.* **1934**, *46*, 618.

(25) Paldus, J.; Čížek, J. *Adv. Quantum Chem.* **1975**, *9*, 105.

(26) Bartlett, R. J.; Purvis, G. D. *Int. J. Quantum Chem.* **1978**, *14*, 516.

(27) Purvis, G. D.; Bartlett, R. J. *J. Chem. Phys.* **1982**, *76*, 1910.

(28) Chan, S. I.; Das, T. P. *J. Chem. Phys.* **1962**, *37*, 1527.

(29) Sadlej, A. J. *Chem. Phys. Lett.* **1975**, *36*, 129.

(30) Lazzaretti, P.; Zanasi, R. *J. Chem. Phys.* **1980**, *72*, 6768.

(31) Kutzelnigg, W. *Isr. J. Chem.* **1980**, *19*, 193.

(32) Schindler, M.; Kutzelnigg, W. *J. Chem. Phys.* **1982**, *76*, 1919.

(33) van Wüllen, C.; Kutzelnigg, W. *Chem. Phys. Lett.* **1993**, *205*, 563.

(34) Hansen, A. E.; Bouman, T. D. *J. Chem. Phys.* **1985**, *82*, 5035.

(35) London, F. *J. Phys. Radium* **1937**, *8*, 397.

(36) Bak, K. L.; Jørgensen, P.; Helgaker, T.; Ruud, K.; Jensen, H. J. A. *J. Chem. Phys.* **1993**, *98*, 8873.

(37) Hameka, H. F. *Mol. Phys.* **1958**, *1*, 203.

(38) Hameka, H. F. *Z. Naturforsch., A: Phys. Sci.* **1959**, *14*, 599.

(39) Hameka, H. F. *Rev. Mod. Phys.* **1962**, *34*, 87.

(40) Ditchfield, R. *J. Chem. Phys.* **1972**, *56*, 5688.

(41) Wolinski, K.; Hinton, J. F.; Pulay, P. *J. Am. Chem. Soc.* **1990**, *112*, 8251.

(42) Häser, M.; Ahlrichs, R.; Baron, H. P.; Weis, P.; Horn, H. *Theor. Chim. Acta* **1992**, *83*, 455.

(43) Gauss, J. *Chem. Phys. Lett.* **1992**, *191*, 614.

(44) Ruud, K.; Helgaker, T.; Bak, K. L.; Jørgensen, P.; Jensen, H. J. A. *J. Chem. Phys.* **1993**, *99*, 3847.

(45) Gauss, J.; Stanton, J. F. *J. Chem. Phys.* **1995**, *103*, 3561.

(46) Gauss, J.; Stanton, J. F. *J. Chem. Phys.* **1996**, *104*, 2574.

(47) Gauss, J. *J. Chem. Phys.* **2002**, *116*, 4773.

(48) Wilson, P. J.; Amos, R. D.; Handy, N. C. *THEOCHEM* **2000**, *506*, 335.

(49) Mohn, C. E.; Wilson, D. J. D.; Lutnæs, O. B.; Helgaker, T.; Ruud, K. *Adv. Quantum Chem.* **2005**, *50*, in press.

(50) *DALTON, a Molecular Electronic Structure Program*, release 2.0; 2005. see http://www.kjemi.uio.no/software/dalton/dalton.html.

(51) Olsen, J.; Jørgensen, P. *J. Chem. Phys.* **1985**, *82*, 3235.

(52) Helgaker, T.; Wilson, P. J.; Amos, R. D.; Handy, N. C. *J. Chem. Phys.* **2000**, *113*, 2983.

(53) Helgaker, T.; Watson, M.; Handy, N. C. *J. Chem. Phys.* **2000**, *113*, 9402.

(54) Helgaker, T.; Pecul, M. In *Calculation of NMR and EPR Parameters. Theory and Applications*; Kaupp, M., Bühl, M., Malkin, V. G., Eds.; Wiley-VCH: Weinheim, Germany, 2004.

(55) Lantto, P.; Vaara, J.; Helgaker, T. *J. Chem. Phys.* **2002**, *117*, 5998.

(56) Lutnæs, O. B.; Ruden, T. A.; Helgaker, T. *Magn. Reson. Chem.* **2004**, *42*, S117.

(57) Keal, T. W.; Tozer, D. J. *J. Chem. Phys.* **2003**, *119*, 3015.

(58) Keal, T. W.; Tozer, D. J.; Helgaker, T. *Chem. Phys. Lett.* **2004**, *391*, 374.

(59) Keal, T. W.; Tozer, D. J. *J. Chem. Phys.* **2004**, *121*, 5654.

(60) Amos, R. D.; Alberts, I. L.; Andrews, J. S.; Colwell, S. M.; Handy, N. C.; Jayatilaka, D.; Knowles, P. J.; Kobayashi, R.; Laidig, K. E.; Laming, G.; Lee, A. M.; Maslen, P. E.;

Murray, C. W.; Rice, J. E.; Simandiras, E. D.; Stone, A. J.; Su, M.-D.; Tozer, D. J. *CADPAC, the cambridge analytic derivatives package*, issue 6; University of Cambridge: Cambridge, U. K., 2005.

(61) Kendall, R. A.; Dunning, T. H., Jr.; Harrison, R. J. *J. Chem. Phys.* **1992**, *96*, 6796.

(62) Dunning, T. H., Jr. *J. Chem. Phys.* **1989**, *90*, 1007.

(63) de Leeuw, F. H.; Dymanus, A. *Chem. Phys. Lett.* **1970**, *7*, 288.

(64) Ellenbroek, A. W.; Dymanus, A. *Chem. Phys. Lett.* **1976**, *42*, 303.

(65) Meerts, W. L.; Stolte, S.; Dymanus, A. *Chem. Phys.* **1977**, *19*, 467.

(66) Reinartz, J. M. L. J.; Meerts, W. L.; Dymanus, A. *Chem. Phys.* **1980**, *45*, 387.

(67) Ruud, K.; Skaane, H.; Helgaker, T.; Bak, K. L.; Jørgensen, P. *J. Am. Chem. Soc.* **1994**, *116*, 10135.

(68) NIST Computational Chemistry Comparison and Benchmark Database, NIST Standard Reference Database Number 101, release 11. http://srdata.nist.gov/cccbdb (May, 2005).

(69) Maroulis, G.; Pouchan, C. *Chem. Phys.* **1997**, *215*, 67.

(70) LeGuennec, M.; Wlodarczak, G.; Demaison, J.; Büurger, H.; Litz, M.; Willner, H. *J. Mol. Spectrosc.* **1993**, *157*, 419.

(71) O'Neill, D. P.; Gill, P. M. W. *Mol. Phys.* **2005**, *103*, 763.

(72) Puzzarini, C. *Phys. Chem. Chem. Phys.* **2004**, *6*, 344.

(73) Maroulis, G. *J. Comput. Chem.* **2003**, *24*, 443.

(74) Margules, L.; Demaison, J.; Rudolph, H. D. *J. Mol. Struct.* **2001**, *599*, 23.

(75) Nakata, M.; Kohata, K.; Fukuyama, T.; Kuchitzu, K.; Wilkins, C. J. *J. Mol. Spectrosc.* **1980**, *68*, 271.

(76) Harmony, M. D.; Kuczkowski, R. W. L. R. L.; Schwendemann, R. H.; Ramsay, D. A.; Lovas, F. J.; Lafferty, W. J.; Maki, A. G. *J. Phys. Chem. Ref. Data* **1979**, *8*, 619.

(77) Huisman, P. A. G.; Klebe, K. J.; Mijlhoff, F. C.; Renes, G. H. *J. Mol. Struct.* **1979**, *57*, 71.

(78) Mom, V.; Huisman, P. A. G.; Mijlhoff, F. C.; Renes, G. H. *J. Mol. Struct.* **1980**, *62*, 95.

(79) Staley, S. W.; Norden, T. D.; Taylor, W. H.; Harmony, M. D. *J. Am. Chem. Soc.* **1987**, *109*, 7641.

CT050101T